


RESEARCH

Open Access



ATP11B triggers the infiltration of T cells into GBM and intensifies anti-GBM immunity by upregulating and externalizing S1PR1

Hui Qiu^{1,2†}, Ziqin Chen^{1,3†}, Jie Chen^{1,2†}, Huijuan Yu³, Xin Wen^{1,2}, Chang Xu¹, Gongzhen Liu¹, Luyijie Chai¹, Longzhen Zhang^{1,2}, Yilong Guo^{1,4*} and Xin Ding^{1,2*} 

Abstract

Background Insufficient T-cell infiltration in tumours causes immune checkpoint inhibitor (ICI) resistance in glioblastoma (GBM) patients. The aim of this study was to demonstrate a preferable way to facilitate T-cell infiltration and improve the therapeutic effects of ICIs in GBM.

Methods Flow cytometry, western blot and immunofluorescence staining were used to detect the effects of ATP11B upregulation on S1PR1 expression and distribution, T-cell infiltration and differentiation. A coculture system and an intracranial GBM model were established to explore the anti-GBM potential of ATP11B/S1PR1 signaling through systemic administration of CD3-DSPE-PEG2K-NHS/ATP11B nanoparticles to specifically deliver ATP11B overexpressing plasmids to T cells.

Results S1PR1 deficiency in T cells caused T-cell lymphopenia and systemic immunosuppression in GBM, whereas ATP11B overexpression induced the upregulation and externalization of S1PR1 on T-cell membranes, thus increasing the ability of T cells to eliminate GBM cells. In intracranial GBM models, an ATP11B overexpression plasmid was specifically delivered to T cells in the peripheral blood, bone marrow and spleen, then triggering the infiltration of T cells deeply into the GBM and reversing systemic immunosuppression, ultimately enhancing the therapeutic outcomes of ICIs.

Conclusions The upregulation and externalization of S1PR1 on T cells mediated by ATP11B overexpression may be promising immunotherapeutic alternatives for GBM treatment.

Keywords Glioblastoma, ATP11B, S1PR1, T-cell lymphopenia, Immune checkpoint inhibitor resistance

[†]Hui Qiu, Ziqin Chen and Jie Chen contributed equally to this work.

*Correspondence:

Yilong Guo
guoyilong888@163.com
Xin Ding
dingxin81@163.com

¹Cancer Institute, Xuzhou Medical University, Jiangsu, Xuzhou 221000, China

²Department of Radiation Oncology, Affiliated Hospital of Xuzhou Medical University, Xuzhou 221000, Jiangsu, China

³Department of Radiation Oncology, Affiliated Huai'an Hospital of Yangzhou University, Huai'an Fifth People's Hospital, Huai'an 223300, Jiangsu, China

⁴Department of Radiation Oncology, Affiliated Pizhou Hospital of Xuzhou Medical University, Xuzhou 221300, Jiangsu, China



© The Author(s) 2025. **Open Access** This article is licensed under a Creative Commons Attribution-NonCommercial-NoDerivatives 4.0 International License, which permits any non-commercial use, sharing, distribution and reproduction in any medium or format, as long as you give appropriate credit to the original author(s) and the source, provide a link to the Creative Commons licence, and indicate if you modified the licensed material. You do not have permission under this licence to share adapted material derived from this article or parts of it. The images or other third party material in this article are included in the article's Creative Commons licence, unless indicated otherwise in a credit line to the material. If material is not included in the article's Creative Commons licence and your intended use is not permitted by statutory regulation or exceeds the permitted use, you will need to obtain permission directly from the copyright holder. To view a copy of this licence, visit <http://creativecommons.org/licenses/by-nc-nd/4.0/>.

Background

T-cell lymphopenia and T-cell dysfunction, which facilitate resistance to immune checkpoint inhibitors (ICIs), are particularly severe in patients with glioblastoma (GBM) [1–3]. Previous studies have demonstrated that a large proportion of T cells are sequestered in the bone marrow of patients with GBM or brain metastases, which is accompanied by the tumour-imposed loss of sphingosine 1-phosphate receptor-1 (S1PR1) from the surface of T cells and is reversible upon holding back S1PR1 internalization [2, 4]. Moreover, S1PR1 and its ligand sphingosine-1-phosphate (S1P) facilitate T-cell differentiation into Th1/Th17 cells but not regulatory T cells (Tregs), and the S1P/S1PR1 pathway participates in modulating the activities of CD4⁺ and CD8⁺ T cells [5]. Therefore, upregulating S1PR1 expression and promoting the externalization of S1PR1 on T-cell membranes are expected to trigger T-cell infiltration into GBM lesions and elicit anti-GBM immunity.

ATPase phospholipid transporting 11B (ATP11B), an ATP-dependent flippase belonging to the subfamily of type 4 P-type ATPases, is widely expressed on cell membranes [6]. Previous studies have demonstrated that low ATP11B expression is associated with poor prognosis and enhanced metastasis in cancer patients [7], and ATP11B is heterogeneously expressed in various nerve cells in the brain [8], suggesting that ATP11B is closely related to the field of neurology or oncology, especially neurological oncology. In addition, the deletion of ATP11B which triggers phosphatidylserine externalization induces a global immunosuppressive signal and mediates immune escape in cancers [9]. Consequently, we hypothesized that the overexpression of ATP11B could facilitate the extracellular localization of the S1PR1 protein on the membranes of T cells, thereby promoting the infiltration of T lymphocytes into GBM and improving the antitumour effects of ICIs.

To efficiently and specifically deliver the ATP11B overexpression (ATP11B-OE) plasmid into T cells, the ATP11B-OE plasmid must be encapsulated in a carrier system with T-cell-specific targeting that can protect the plasmid from degradation by nuclease activity. Among all vector systems, cationic liposome nanoparticles (NPs) represent the most advanced platform for drug delivery to the brain [10]. Furthermore, targeting T cells with a CD3-specific antibody provides a satisfactory approach for achieving specific T cell transfection [11–14]. In this study, cationic liposome NPs conjugated with a CD3 targeting monoclonal antibody named CD3-DSPE-PEG2K-NHS/ATP11B were synthesized to transfect ATP11B-OE plasmids into T cells. We found that ATP11B upregulation significantly enhanced the expression and extracellular localization of the S1PR1 protein on T cells, which then promoted T lymphocyte infiltration into GBM

lesions, induced T cells to polarize towards anti-tumour phenotypes and reversed systemic immunosuppression. Encouragingly, the systemic administration of CD3-DSPE-PEG2K-NHS/ATP11B NPs enhanced the therapeutic outcomes of radiotherapy (RT) combined with ICIs in murine models of intracranial GBM. Overall, the specific upregulation and externalization of the S1PR1 protein on T-cell membranes mediated by ATP11B upregulation represents a promising immunotherapeutic adjunct for GBM treatment.

Methods

Cell lines

The GBM cell lines GL261 and G422, the T-cell line Jurkat, and microglia BV2 were obtained from the Cell Bank, Chinese Academy of Sciences (Shanghai, China). GL261, G422 and BV2 cells were cultured in Dulbecco's modified Eagle's medium (HyClone, Logan, USA), and Jurkat cells were cultured in Roswell Park Memorial Institute-1640 medium (HyClone, Logan, USA). The culture medium was supplemented with 10% foetal bovine serum (FBS; HyClone, Logan, USA). The cells were grown in humidity with 5% CO₂ at 37 °C.

Establishment of intracranial GBM models and subcutaneous GBM models

Male C57BL/6J mice, aged 6 to 8 weeks, were purchased from GemPharmatech (Nanjing, China) and acclimated in a specific pathogen-free environment for at least one week before in vivo experiments were conducted.

For subcutaneous implantation, 1×10^7 GBM cells per mouse were delivered in a total volume of 100 µL of phosphate-buffered saline (PBS) into the subcutaneous dorsal region of each mouse, and the tumour size and body weight were recorded every 3 days. The rodent health endpoints were determined by the rupture of subcutaneous tumours, 20% weight loss, a tumour size exceeding 20 mm or the appearance of abnormal central neurological symptoms.

For intracranial implantation, 8×10^5 luciferase-labelled GBM cells per mouse were delivered in a total volume of 5 µL of PBS into the brain via a stereotactic frame, and the implant site was located 2 mm to the right of the bregma and 3 mm below the surface of the skull at the coronal suture. Seven days after implantation, the intracranial tumours were detected via a small animal live imaging system, and the rodent health endpoints were natural death, 20% weight loss or the appearance of abnormal central neurological symptoms.

Cell phenotype detection by flow cytometry

After being euthanized with excess carbon dioxide, the peripheral blood of the mice was collected, the bone marrow was gently extracted, and the spleen tissues

were ground. Red blood cells were then removed with BD Pharm Lyse™ lysis buffer (BD Biosciences, New Jersey, USA). After counting the abovementioned cell suspensions and Jurkat cells cultured in vitro, the same number of single cells were then fixed and permeabilized according to the manufacturer's protocol for the BD Cytofix/Cytoperm™ fixation/permeabilization kit (BD Biosciences, New Jersey, USA). The cells were subsequently incubated with the following corresponding antibodies conjugated with different fluorochromes: S1PR1 polyclonal antibody+Alex Fluor 488-conjugated anti-rabbit IgG(H+L), APC-conjugated anti-human CD3 (OKT3), FITC-conjugated anti-mouse CD3 (17A2), FITC-conjugated anti-human CD4 (OKT4), APC-conjugated anti-human CD4 (OKT4), APC-conjugated anti-mouse CD4 (GK1.5), APC-conjugated anti-mouse CD8a (53-6.7), APC-conjugated anti-human CD8a (RPA-T8), T-bet polyclonal antibody+Texas red-conjugated anti-rabbit IgG(H+L) or Alex Fluor 488-conjugated anti-rabbit IgG(H+L), GATA3 monoclonal antibody+PE-conjugated anti-mouse IgG(H+L), FOXP3 polyclonal antibody+Alex Fluor 488-conjugated anti-rabbit IgG(H+L) or PE-conjugated anti-rabbit IgG(H+L) (1:300; Protein Technology, Wuhan, China) for 30 min at 4 °C in the dark. The cells were washed with PBS by centrifugation at 500×g for 5 min, resuspended in staining buffer, and then analysed via a flow cytometer (BD Biosciences, New Jersey, USA). The populations of Th1 cells, Th2 cells and Tregs were defined among the CD4⁺ T cells. The experiment was independently repeated at least three times.

Cell transfection assay

The ATP11B-OE plasmid and negative control (NC) plasmid were synthesized by Miaoling Biology Co.Ltd. (Hubei, China). Three ATP11B-targeting small interfering RNAs (siATP11B) and NC siRNA were obtained from Sangon Biotech Co., Ltd. (Shanghai, China), and their sequences are shown in Table 1. Cell transfection was conducted with Lipo6000™ transfection reagent (Beyotime, Shanghai, China) following the manufacturer's protocol.

Table 1 The sequences of siATP11B and siNC

Gene name	Sense (5'-3')	Antisense (5'-3')
siATP11B#1	CGUAGGAGAAUGAGUGUAAUUTT	AAUUACACUCAUUCUCCUACGTT
siATP11B#2	GCCAACUUGGACAGUCUCAUATT	UAUGAGACUGUC-CAAGUUGGCTT
siATP11B#3	GCUGCAAGAAACAGUGACUAUTT	AUAGUCACU-GUUUCUUGCAGCTT
NC	UUCUCCGAACGUGUCACGUTT	ACGUGACACGUUCGGAGAATT

Cell counting Kit-8 (CCK-8) assay

The cells were incubated at a suitable density in 96-well plates and cultured for 12 h. Then, the cells were transfected with the ATP11B-OE plasmid or the NC plasmid. After being cultured for another 24 h, 48 h, or 72 h, CCK-8 solution was added, and the mixture was incubated for 2 h. The optical density (OD) values were measured at 450 nm via a microplate reader (BioTek, Vermont, USA). The experiment was independently repeated three times.

Western blot

Total cellular proteins were extracted via RIPA lysis buffer (Beyotime, Shanghai, China) and separated via 10% sodium dodecyl sulfate-polyacrylamide gel electrophoresis (New Cell & Molecular Biotech, Suzhou, China). The isolated proteins were transferred to polyvinylidene difluoride membranes (Millipore, Boston, USA) and blocked with 5% skim milk (VICMED, Xuzhou, China) for 1 h at room temperature. The membranes were subsequently incubated with anti-ATP11B, anti-S1PR1, anti-CD68, anti-CD80, anti-CD206, anti-γ-H₂AX, anti-β-actin or anti-GAPDH antibodies (1:1000; Protein Technology, Wuhan, China) overnight at 4 °C. The membranes were then incubated with horseradish peroxidase-labelled secondary antibodies corresponding to the primary antibody species for 45 min at room temperature. After washing, the protein bands were visualized via an enhanced chemiluminescence (ECL) kit (New Cell & Molecular Biotech, Suzhou, China) and chemiluminescence imaging system (Tanon, Shanghai, China). The experiment was independently repeated at least three times.

Cell apoptosis assay

Jurkat cells were transfected with ATP11B-OE or NC plasmid, and 24 h later, the transfected Jurkat cells were cocultured with GL261 or G422 cells, respectively, for another 6 h or 24 h. Then the suspended Jurkat cells were removed by washing, and the GL261 and G422 cells were collected and analysed for apoptosis via flow cytometry (BD Biosciences, New Jersey, USA) with an Annexin V-FITC/PI apoptosis detection kit (KEYGEN Biotech, Nanjing, China). The experiment was independently repeated three times.

Cell migration assay

A cell migration assay was conducted using a Transwell chamber with a 5 μm pore size (Corning, New York, USA). First, Jurkat cells were transfected with ATP11B-OE or NC plasmid for 48 h and labelled with a DiI cell membrane staining kit (Beyotime, Shanghai, China). Jurkat cells were subsequently seeded in the upper chamber, and green fluorescent protein (GFP)-labelled GL261 or G422 cells were seeded in the lower chamber.

After coculture for 6 h or 24 h, fluorescence images were captured and quantified via a fluorescence microscope (Olympus, Tokyo, Japan). The experiment was independently repeated three times.

Construction and characterization of CD3-DSPE-PEG2K-NHS/ATP11B NPs

1,2-Distearoyl-sn-glycero-3-phosphoethanolamine-polyethylene glycol 2000-N-hydroxysuccinimide (DSPE-PEG2K-NHS) (Ruixi Biological Technology, Xi'an, China) was solubilized in absolute ethanol (Sinopharm Chemical Reagent, Shanghai, China), and a CD3 monoclonal antibody (MedChemExpress, New Jersey, USA) was conjugated with DSPE-PEG2K-NHS according to the instructions provided by the phospholipid conjugation kit (Ruixi Biological Technology, Xi'an, China) at a molar ratio of 1:1. Absolute ethanol-dissolved 1,2-dioleoyl-3-trimethylammonium propane (DOTAP), dioleoylphosphatidylethanolamine (DOPC) and cholesterol (Chol) were then mixed with CD3-DSPE-PEG2K-NHS at a molar ratio of 4:1:4:1. The mixture was vortexed continuously for 5 min at room temperature, and dialyzed in diethylpyrocarbonate-treated distilled water for 3 h in a dialysis bag (Solarbio, Beijing, China) to remove impurities. The compound in the dialysis bag was recovered as the synthesized CD3-DSPE-PEG2K-NHS cationic liposomes and stored at room temperature.

According to the different N/P molar ratios, appropriate amounts of ATP11B-OE plasmid solution were gently added to the CD3-DSPE-PEG2K-NHS cationic liposomes solution. After gentle mixing, the mixture was incubated at room temperature for 15 min to construct CD3-DSPE-PEG2K-NHS/ATP11B. The optimal N/P ratio was then selected via agarose gel electrophoresis. Briefly, a 2% agarose gel was prepared and samples of the ATP11B-OE plasmid and CD3-DSPE-PEG2K-NHS/ATP11B were separately added to the bottom of the wells. After electrophoresis for 15 min at 120 V, the DNA fragments were visualized via an ultraviolet gel image analysis system (Tanon, Shanghai, China).

The particle size and zeta potential of CD3-DSPE-PEG2K-NHS cationic liposomes and CD3-DSPE-PEG2K-NHS/ATP11B were determined via dynamic light scattering via a Malvern Zetasizer (Worcestershire, United Kingdom) at 25 °C.

Therapeutic regimen for intracranial GBM models

For detection of therapeutic effects *in vivo*, when an intracranial tumour fluorescence signal appeared, the mice were randomly divided into the following eight groups (eight mice per group): the control group, PD-1 inhibitor group, CD3-DSPE-PEG2K-NHS/ATP11B group, RT group, RT + PD-1 inhibitor group, RT + CD3-DSPE-PEG2K-NHS/ATP11B group, PD-1

inhibitor + CD3-DSPE-PEG2K-NHS/ATP11B group, and RT + PD-1 inhibitor + CD3-DSPE-PEG2K-NHS/ATP11B group. Whole-brain RT (3 Gy/fraction/day×3 days) was used with the remaining parts of the body shielded with lead blocks; PBS, PD-1 inhibitor (200 µg/mouse/day×3 days) and CD3-DSPE-PEG2K-NHS/ATP11B (ATP11B plasmid: 1 µg/g body weight/day×1 day) were administered through the tail vein. On days 5 and 10, the orthotopic GBM-bearing mice were fluorescently imaged again. Three mice per group were selected for the collection of peripheral blood, brain tissue and other normal organ tissues including heart, liver, spleen, lung, and kidney, while another five mice per group were observed to record overall survival (OS) times, after which Kaplan-Meier survival curves were plotted.

Immunofluorescence staining

Freshly collected brain tissues were fixed with 4% paraformaldehyde for 48 h to prepare frozen sections (thickness = 5 µm). After recovering to room temperature, the sections were boiled in 0.01 M citrate buffer (pH = 6.0; Servicebio, Wuhan, China), covered with 3% hydrogen peroxide solution (Caoshanhu, Nanchang, China) and permeabilized with 0.5% Triton X-100 (Thermo Scientific, Massachusetts, USA). The sections were subsequently blocked with 10% bovine serum albumin solution (Vicmed, Xuzhou, China) for 45 min and stained with anti-CD3, anti-CD4, anti-CD8 or anti-FOXP3 antibodies (Protein Technology, Wuhan, China) at a dilution of 1:500 overnight at 4 °C. After being washed with PBS, the sections were then stained with CoraLite488-conjugated goat anti-rabbit IgG or Alexa Fluor555-conjugated goat anti-mouse IgG (Proteintech, Wuhan, China) at a dilution of 1:500 at room temperature for 40 min in the dark. Finally, the sections were washed with PBS, followed by staining with 4',6-diamidino-2-phenylindole dihydrochloride for 5 min at room temperature in the dark. Fluorescence images were captured using an Olympus BX53 fluorescence microscope (Tokyo, Japan).

Hematoxylin-eosin (H&E) staining assay

Paraffin sections of heart, liver, spleen, lung, and kidney tissues were prepared and deparaffinized via xylene (Sinopharm Chemical Reagent, Shanghai, China) and hydrated with gradient alcohol (Sinopharm Chemical Reagent, Shanghai, China) and double distilled water. The sections were subsequently stained with hematoxylin, differentiated with differentiation solution and stained with eosin according to the instructions provided with the H&E staining kit (Solarbio, Beijing, China). The tissue sections were sealed with neutral balsam (Vicmed, Xuzhou, China) and scanned via slide scanning microscopy (Olympus, Tokyo, Japan).

Statistical analysis

Statistical analysis was performed with GraphPad Prism 8.0 (San Diego, USA), and the data are presented as the means \pm standard deviations. Two-tailed Student's *t* tests were used to analyse the significant differences between two groups, and survival analysis was performed via Kaplan-Meier survival curves and the log-rank test. **P* < 0.05, ***P* < 0.01, and ****P* < 0.001.

Results

Loss of S1PR1 on T cells caused CD4⁺ and CD8⁺ T-cell lymphopenia in GBM

To investigate the effects of intracranial tumours on the systemic immune microenvironment, we established two murine GBM models: an intracranial GBM model in which luciferase-labelled GL261 cells were injected into the specific brains of C57BL/6J mice and a subcutaneous GBM model in which GL261 cells were injected into the dorsal region of C57BL/6J mice. Twenty days later, the peripheral blood of the tumour-bearing mice was collected and analysed. Compared with the subcutaneous GBM model, the intracranial GBM model exhibited significant CD4⁺ T-cell lymphopenia and CD8⁺ T-cell lymphopenia (all *P* < 0.001), and the expression level of T-bet (a marker for Th1 cells) also decreased but did not reach statistical significance (Fig. 1A and B). Furthermore, the

expression levels of GATA-3 (a marker for Th2 cells) and FOXP3 (a marker for Tregs) were significantly increased (all *P* < 0.001) in the mice bearing intracranial tumours (Fig. 1A and B). These results suggest that intracranial tumours cause stronger systemic immunosuppression.

A previous study revealed that T cells are sequestered in the bone marrow in the setting of GBM, which is associated with the loss of surface S1PR1 expression [2]. We subsequently detected the surface S1PR1 levels on T cells in the peripheral blood of intracranial GBM-bearing mice via flow cytometry. The results revealed markedly lower levels of surface S1PR1 on T cells in the intracranial GBM model than in the subcutaneous GBM model (Fig. 1C and D). Therefore, increasing the surface S1PR1 level on T cells is expected to reverse the systemic immunosuppression of GBM.

ATP11B overexpression induced the upregulation and membrane externalization of the S1PR1 protein

To externalize the membrane-expressed S1PR1 protein, we overexpressed the flippase ATP11B protein. The ATP11B-OE plasmid was transferred into GBM cell lines (GL261 and G422) and Jurkat cells, and the results revealed that, compared with those in the NC group, the expression levels of the ATP11B and S1PR1 proteins in the ATP11B-OE group were significantly increased 48 h

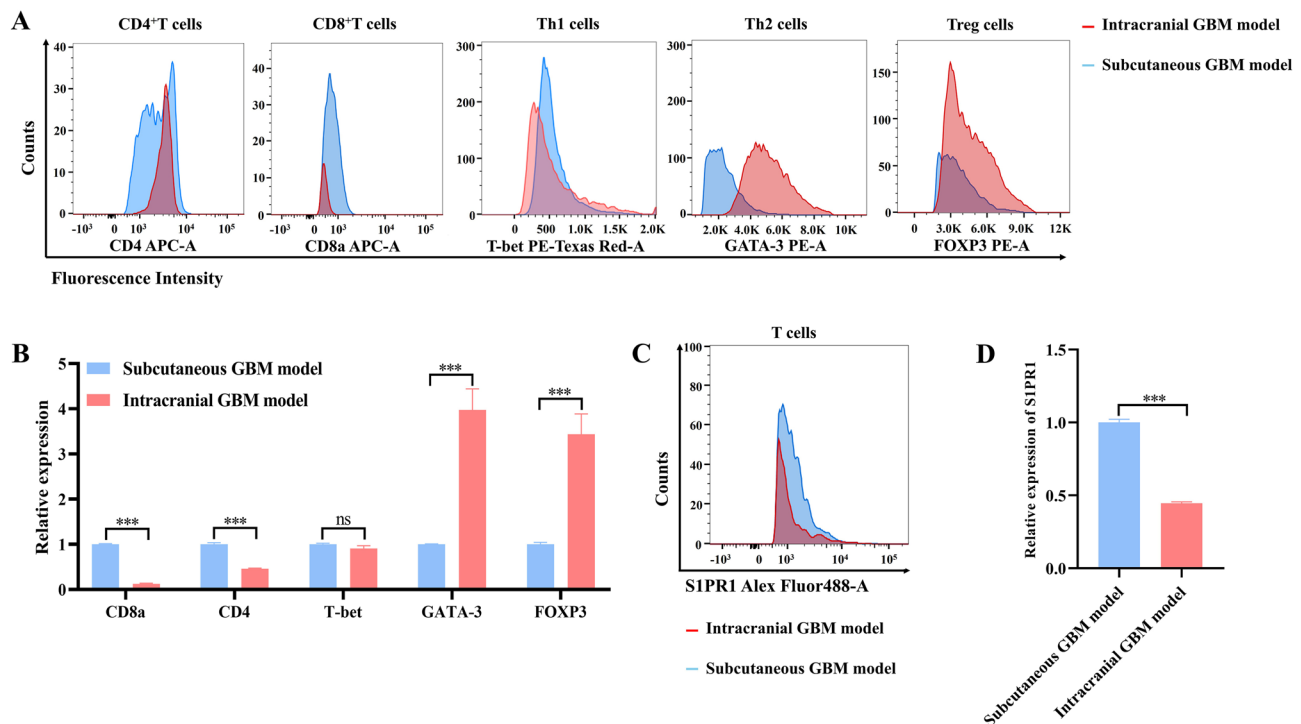


Fig. 1 Loss of S1PR1 on T cells caused systemic immunosuppression in murine intracranial GBM model. Two murine GBM models were established through the intracranial or subcutaneous injection of luciferase-labelled GL261 cells. Twenty days later, peripheral blood samples were collected to detect the T-lymphocyte subsets (including CD4⁺ T cells, CD8⁺ T cells, Th1 cells, Th2 cells and Tregs) (**A**) and the levels of surface S1PR1 protein on T cell membranes (**C**) via flow cytometry, and the results are presented in the corresponding representative experiment. The statistical analysis of three independently duplicated datasets derived from A and C is presented in (**B**) and (**D**), respectively

after transfection (Fig. 2A to C), whereas the ATP11B and S1PR1 proteins exhibited synchronous decreases following interference with ATP11B protein expression (Fig. 2D). Additionally, the membrane externalization level of the S1PR1 protein markedly increased at 48 h after ATP11B-OE plasmid transfection (Fig. 2E). These findings indicate that the upregulation of ATP11B has dual effects, promoting both S1PR1 expression and S1PR1 membrane externalization.

Upregulation and externalization of the S1PR1 protein in T cells induced by ATP11B overexpression intensified the ability of T cells to eliminate GBM cells

Since S1PR1 is involved in the regulation of T-cell differentiation, we subsequently examined the effect of ATP11B overexpression on T-cell differentiation. Flow cytometric analysis revealed that, after being transfected with the ATP11B-OE plasmid for 48 h or 72 h, more CD4⁺ T-lymphocytes and less Tregs were existed in Jurkat^{ATP11B-OE} cells than in Jurkat^{NC} cells (all $P < 0.01$, Fig. 3A and B). In addition, the expression level of Th1 cell marker T-bet increased to a certain extent, whereas the expression level of Th2 cell marker GATA-3 decreased, although the degree of the above changes did not fully reach statistical significance ($P < 0.001$ only for GATA-3 at 72 h after transfection; Fig. 3A and B). These findings suggest that ATP11B overexpression promoted

T lymphocyte differentiation towards antitumour phenotypes.

To directly assess the effect of Jurkat cells transfected with the ATP11B-OE plasmid on the proliferation of GBM cells, we established a coculture system involving Jurkat cells and GBM cells and then detected the chemotaxis of Jurkat cells to GBM cells and the apoptosis and DNA damage of GBM cells. The results indicated that Jurkat cells overexpressing ATP11B possessed enhanced homing ability towards GBM cells in the microenvironment, which was supported by the evidence that, compared with Jurkat^{NC} cells, Jurkat^{ATP11B-OE} cells exhibited more significant localization around GL261 cells with a statistically significant increase in the number of Jurkat^{ATP11B-OE} cells in the lower chamber after 1 h of coculture (Fig. 3C and E). Moreover, Jurkat^{ATP11B-OE} cells induced greater apoptosis of cocultured GBM cells than Jurkat^{NC} cells did, with even more significant apoptosis observed after 24 h of coculture ($P < 0.05$, Fig. 3F and G). To detect the effect of T cells overexpressing ATP11B on DNA damage in cocultured GBM cells, total protein from GBM cells cocultured with Jurkat^{ATP11B-OE} or Jurkat^{NC} cells for 24 h was extracted and then exposed to an anti- γ -H₂AX antibody. As shown in Fig. 3H, compared with that in Jurkat^{NC} cells, the expression of γ -H₂AX was significantly elevated in GL261 and G422 cells cocultured with Jurkat^{ATP11B-OE} cells.

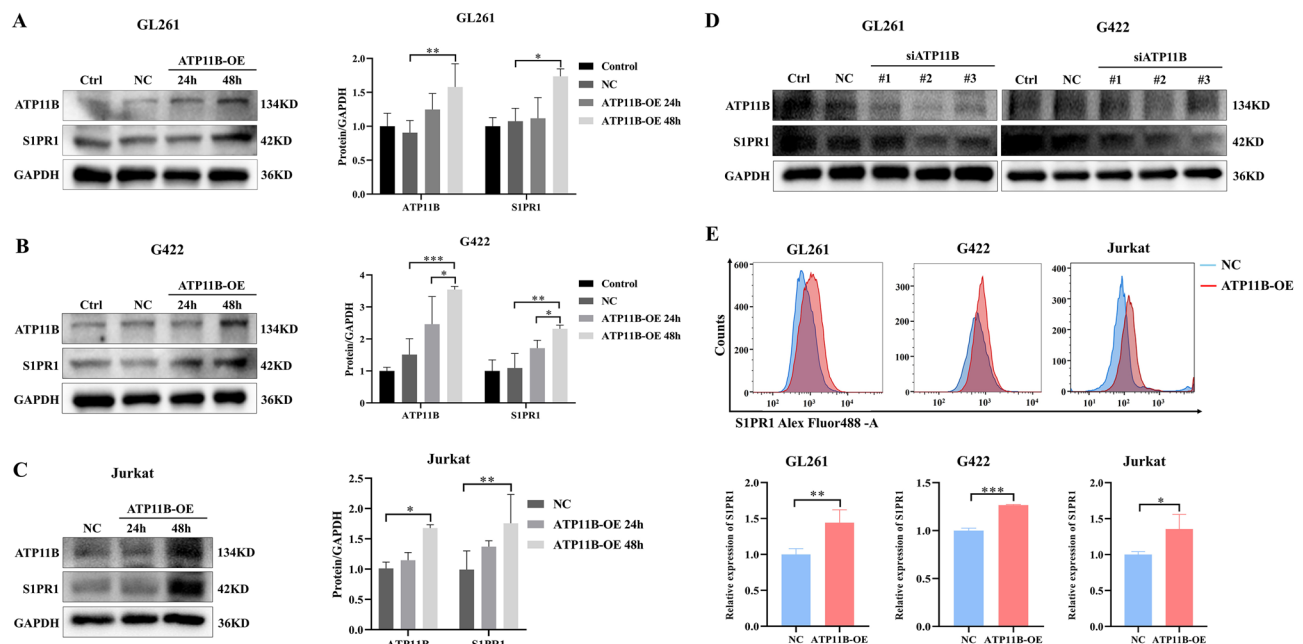


Fig. 2 ATP11B overexpression induced the upregulation and membrane externalization of the S1PR1 protein in cells. The ATP11B-OE plasmid was transferred into GBM cell lines (GL261 and G422) and Jurkat cells for 24 h and 48 h. The expression levels of ATP11B and S1PR1 in GL261 cells (A), G422 cells (B) and Jurkat cells (C) were detected via western blot, and their relative expression levels were analysed via three independent experiments. (D) The expression levels of ATP11B and S1PR1 in GL261 and G422 cells 48 h after ATP11B silencing were detected via western blot. (E) Representative flow cytometry image of the surface S1PR1 protein on GL261, G422 and Jurkat cells transfected with the ATP11B-OE plasmid for 48 h, and the relative counts were analysed via three independent experiments

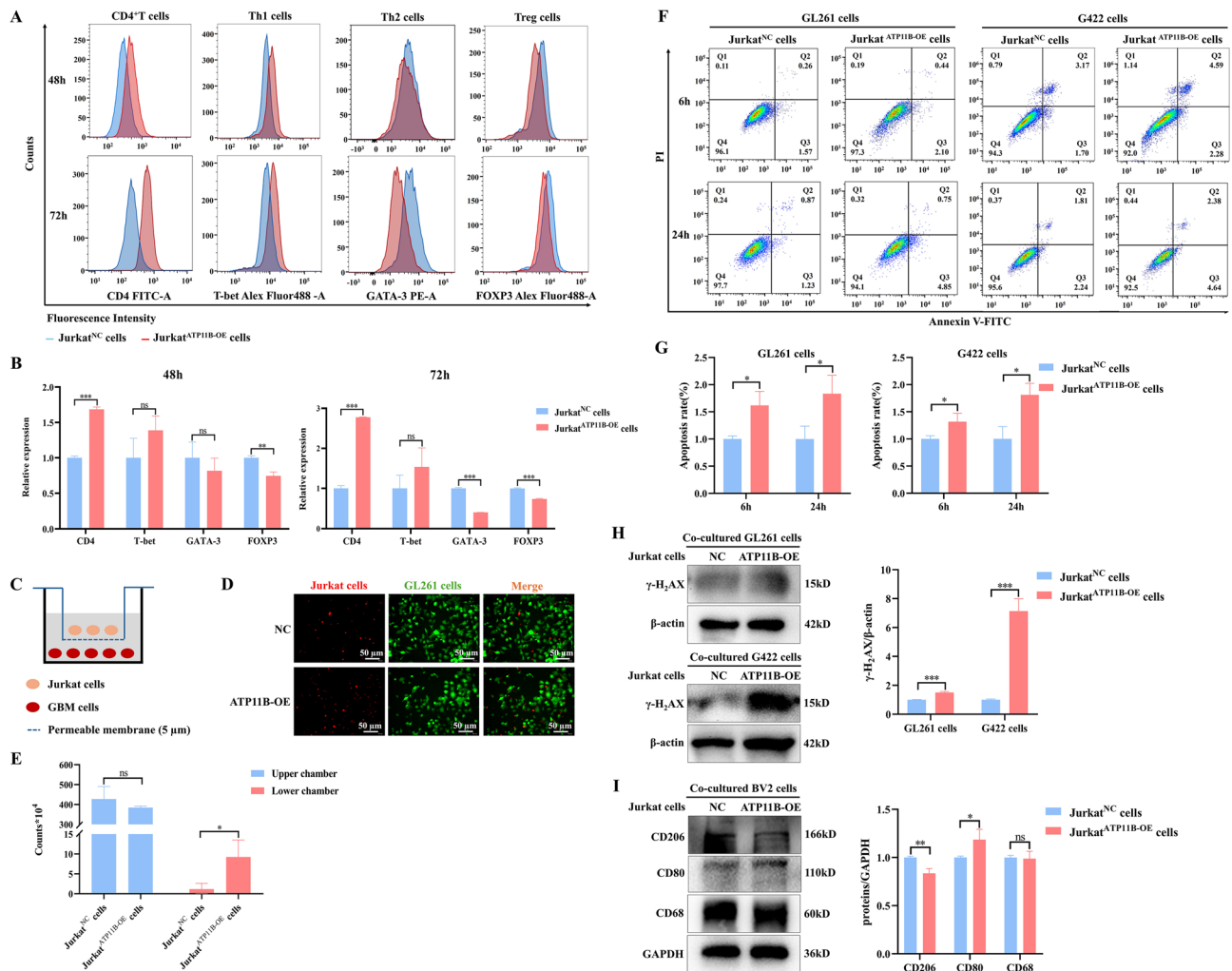


Fig. 3 S1PR1 upregulation and externalization induced by ATP11B overexpression intensified T cells to eliminate GBM cells. **(A)** Representative flow cytometry data of the subsets (including CD4⁺ T cells, Th1 cells, Th2 cells and Tregs) of Jurkat cells transfected with the ATP11B-OE plasmid for 48 h and 72 h. **(B)** Statistical analysis of three independently duplicated datasets derived from A. **(C)** Diagram of the coculture model of GBM cells and Jurkat cells. **(D)** The migration of Jurkat cells (red) to the GBM (green) microenvironment was observed under a fluorescence microscope (scale bar: 50 μm). **(E)** Statistical analysis of the numbers of Jurkat cells in the upper and lower chambers; the experiment was independently performed three times. **(F)** GL261 and G422 cells were cocultured with ATP11B-overexpressing Jurkat cells for 6 h and 24 h, after which flow cytometry was used to detect the apoptosis of GL261 and G422 cells. **(G)** Statistical analysis of the apoptosis rates of cocultured GL261 and G422 cells based on three independent experiments. GL261, G422 and BV2 cells were cocultured with ATP11B-overexpressing Jurkat cells for 24 h, after which western blot was used to detect the expression levels of the DNA damage marker γ-H₂AX **(H)** in GL261 and G422 cells, and the expression levels of CD206, CD80 and CD68 in BV2 cells **(I)**. The expression levels of γ-H₂AX, CD206, CD80 and CD68 were also semiquantitatively analysed in three independent experiments

Because tumour-associated macrophages represent the predominant immune cell type in the GBM microenvironment, constituting approximately 30-50% of tumour cellularity [15, 16], microglia can be classified into proinflammatory M1 and anti-inflammatory M2 phenotypes, and the two phenotypes play distinct roles in cancer progression and suppression [17–19]. Therefore, we detected the influence of ATP11B-overexpressing T cells on the phenotypic differentiation of cocultured BV2 microglia. The results presented in Fig. 3I demonstrated that, compared with Jurkat^{NC} cells, Jurkat^{ATP11B-OE} cells notably

induced cocultured BV2 cells to differentiate into the M1 phenotype while reducing M2 differentiation.

The above results reveal that the membrane externalization of the S1PR1 protein induced by ATP11B overexpression distinctly intensified the ability of T cells to eliminate GBM cells.

Anti-CD3-conjugated NPs efficiently delivered the ATP11B-OE plasmid to T cells distributed in the peripheral blood, bone marrow and spleen

Owing to the susceptibility of plasmids to degradation by nucleases in vivo and the lack of specificity in targeting T

lymphocytes, it is imperative to utilize a vector that can accurately and efficiently deliver plasmids to T lymphocytes. Cationic liposomes are widely recognized for their excellent biocompatibility, stability, ease of modification, and straightforward loading, making them suitable for drug and gene delivery. Consequently, we developed and optimized cationic liposome NPs (CD3-DSPE-PEG2K-NHS/ATP11B) conjugated with a CD3 monoclonal antibody to deliver the ATP11B-OE plasmid specifically to T cells.

We first optimized ATP11B-OE plasmid encapsulation in CD3-DSPE-PEG2K-NHS/ATP11B. The results of agarose gel electrophoresis suggested that when N/P was greater than or equal to 30, CD3-DSPE-PEG2K-NHS cationic liposome could completely encapsulate the ATP11B-OE plasmid (Fig. 4A); therefore, CD3-DSPE-PEG2K-NHS/ATP11B was synthesized under the condition of N/P = 30 and used in subsequent experiments. The particle size distribution and zeta potential were narrow

(PDI < 0.25) and unimodal, with an average diameter of 265.60 ± 5.29 nm and a surface charge of -9.05 ± 0.26 mV at physiological pH (Fig. 4B).

To assess the targeting efficiency of CD3-DSPE-PEG2K-NHS/ATP11B for T cells, Jurkat cells were exposed to PBS, FAM-siRNA, DSPE-PEG2K-NHS/FAM-siRNA or CD3-DSPE-PEG2K-NHS/FAM-siRNA for 6 h or 24 h. As shown in Fig. 4C and D, Jurkat cells in the CD3-DSPE-PEG2K-NHS/FAM-siRNA group presented a significantly greater green fluorescence signal than those in the other three groups did at 6 h ($P < 0.01$), and the difference in green fluorescence intensity was even more pronounced at 24 h ($P < 0.01$), indicating that the CD3-DSPE-PEG2K-NHS cationic liposomes had better T-cell targeting properties. Additionally, we further investigated whether CD3-DSPE-PEG2K-NHS/ATP11B was toxic to T cells, and the results suggested that, compared with the control and CD3-DSPE-PEG2K-NHS/NC, CD3-DSPE-PEG2K-NHS/ATP11B not only was noncytotoxic to

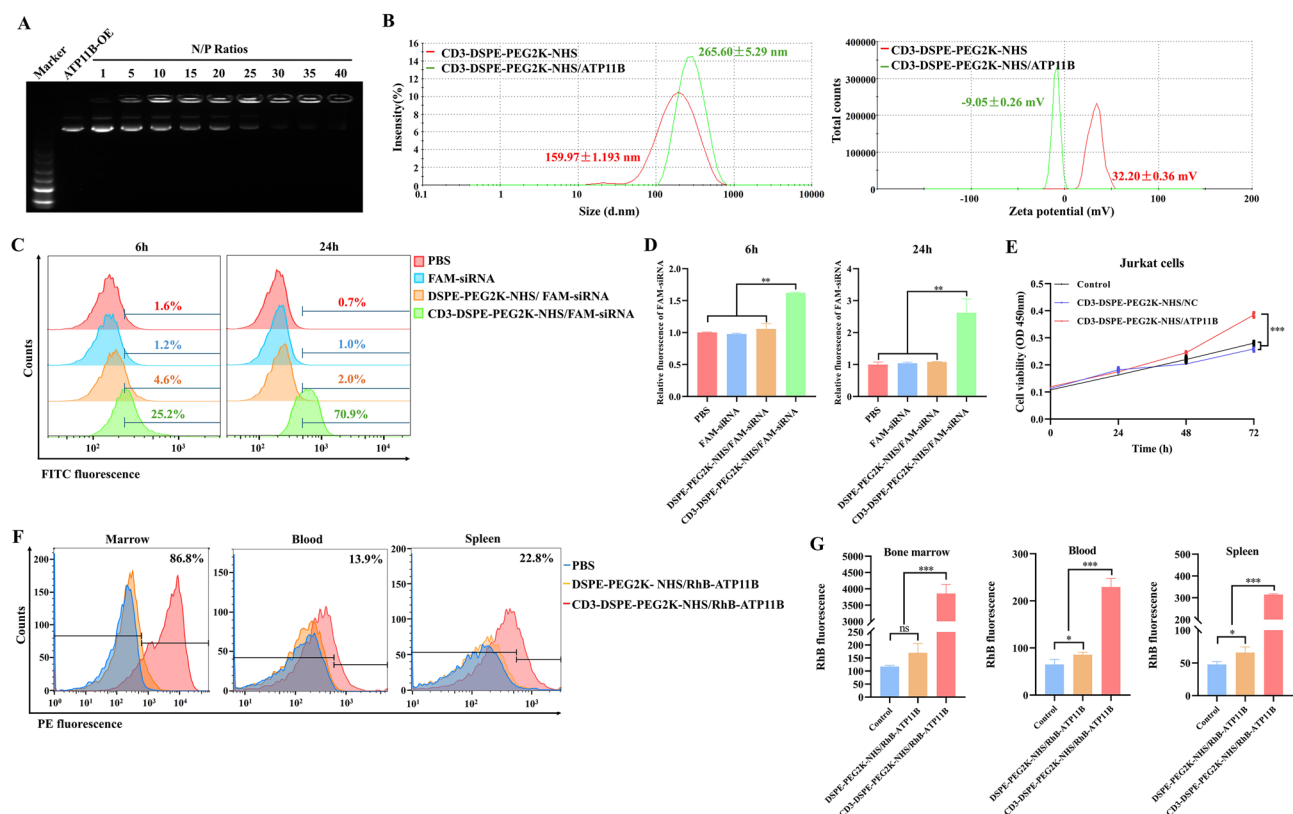


Fig. 4 CD3-DSPE-PEG2K-NHS/ATP11B NPs were successfully synthesized with superior targeting to T cells. **(A)** Agarose gel electrophoresis assay of the binding capacity of the ATP11B-OE plasmid to CD3-DSPE-PEG2K-NHS cationic liposome at various N/P ratios. **(B)** The particle size (left) and zeta-potential (right) of CD3-DSPE-PEG2K-NHS cationic liposome and CD3-DSPE-PEG2K-NHS/ATP11B were detected via dynamic light scattering. **(C)** Jurkat cells were exposed to PBS, FAM-siRNA, DSPE-PEG2K-NHS/FAM-siRNA or CD3-DSPE-PEG2K-NHS/FAM-siRNA for 6 h or 24 h, after which the intensity of green fluorescence in the cells was measured via flow cytometry. **(D)** Statistical analysis of three independently duplicated datasets derived from C. **(E)** Jurkat cells were exposed to PBS, CD3-DSPE-PEG2K-NHS/NC or CD3-DSPE-PEG2K-NHS/ATP11B for 24 h, 48 h or 72 h. Then, the survival of Jurkat cells was detected by a CCK-8 assay, and the experiment was repeated independently three times. **(F)** The RbB-labelled ATP11B-OE plasmid was loaded on DSPE-PEG2K-NHS cationic liposome or CD3-DSPE-PEG2K-NHS cationic liposome and then injected into mice bearing intracranial GBM through the tail vein. 24 h later, T cells in the bone marrow, peripheral blood and spleen samples were collected and measured by flow cytometry to evaluate the red fluorescence intensity. **(G)** Statistical analysis of three independently duplicated datasets derived from F

Jurkat cells but also significantly stimulated their proliferation ($P < 0.001$, Fig. 4E).

To further investigate the targeting efficiency of CD3-DSPE-PEG2K-NHS/ATP11B to T cells, red fluorescent rhodamine B (RhB)-labelled ATP11B-OE plasmids were loaded on CD3-DSPE-PEG2K-NHS cationic liposomes and DSPE-PEG2K-NHS cationic liposomes, and then PBS, DSPE-PEG2K-NHS/RhB-ATP11B and CD3-DSPE-PEG2K-NHS/RhB-ATP11B were injected into the mice via the tail vein independently. 24 h later, T cells in the bone marrow, peripheral blood and spleen samples were collected, and the red fluorescence intensity in the T lymphocytes was detected via flow cytometry to assess the targeting efficiency of the NPs. Compared with those in both the PBS and DSPE-PEG2K-NHS/RhB-ATP11B groups, the red fluorescence intensities of T lymphocytes collected from the bone marrow, peripheral blood and spleen in the CD3-DSPE-PEG2K-NHS/RhB-ATP11B group were significantly greater (all $P < 0.001$, Fig. 4F and G). These findings demonstrate that the CD3-DSPE-PEG2K-NHS/ATP11B NPs efficiently delivered the ATP11B-OE plasmid to T cells distributed in the peripheral blood, bone marrow and spleen *in vivo*.

CD3-DSPE-PEG2K-NHS/ATP11B NPs triggered deep infiltration of T cells into GBM lesions and reversed systemic immunosuppression

We then established an intracranial GBM model and injected CD3-DSPE-PEG2K-NHS/ATP11B NPs through the tail vein. Seven days later, brain tissues and peripheral blood samples were collected for subsequent analysis. After systemic administration of CD3-DSPE-PEG2K-NHS/ATP11B NPs, the expression level of S1PR1 in GBM tissues clearly increased (Fig. 1A). Moreover, while the CD3-DSPE-PEG2K-NHS/NC NPs induced the distribution of most T cells around GBM lesions, the CD3-DSPE-PEG2K-NHS/ATP11B NPs triggered more T cells to infiltrate deeply into the GBM lesions (Fig. 1B). In terms of T-cell phenotypes in the GBM microenvironment, we found that, compared with CD3-DSPE-PEG2K-NHS/NC, CD3-DSPE-PEG2K-NHS/ATP11B NPs induced more CD4⁺ and CD8⁺ T cells to infiltrate the GBM region while reducing the infiltration of Tregs (all $P < 0.05$, Fig. 5C and D).

Moreover, flow cytometry of peripheral blood from orthotopic GBM-bearing mice (Fig. 5E and F) revealed that, compared with tail vein injection of CD3-DSPE-PEG2K-NHS/NC, systemic administration of CD3-DSPE-PEG2K-NHS/ATP11B NPs dramatically promoted the differentiation of T cells into CD4⁺ T cells ($P < 0.01$), CD8⁺ T cells ($P < 0.05$) and Th1 cells ($P < 0.001$), rather than into Th2 cells ($P < 0.01$) and Tregs ($P < 0.001$). These findings suggested that systemic administration of CD3-DSPE-PEG2K-NHS/ATP11B NPs could increase the

anti-GBM activity of immune cells and reverse systemic immunosuppression in GBM.

CD3-DSPE-PEG2K-NHS/ATP11B NPs enhanced the therapeutic outcomes of RT combined with ICIs in GBM

On the basis of the previously detected effects of CD3-DSPE-PEG2K-NHS/ATP11B NPs on the number and phenotypes of T cells, we hypothesized that CD3-DSPE-PEG2K-NHS/ATP11B NPs might improve the anti-GBM efficacy of RT combined with ICIs. In accordance with the flowchart shown in Fig. 6A, we established intracranial GBM models and applied corresponding treatment measures. A small animal live imaging system was regularly used to detect changes in intracranial tumours. The results revealed that systemic administration of CD3-DSPE-PEG2K-NHS/ATP11B NPs restrained the growth of intracranial tumours to a certain extent. Compared with RT or PD-1 inhibitor treatment alone, the addition of CD3-DSPE-PEG2K-NHS/ATP11B NPs further promoted tumour regression; the combination treatment strategy of CD3-DSPE-PEG2K-NHS/ATP11B NPs + RT + PD-1 inhibitor had the strongest anti-GBM effect (Fig. 6B).

After evaluating the treatment response rates, we found that the addition of CD3-DSPE-PEG2K-NHS/ATP11B NPs to the PD-1 inhibitor increased the objective response rate [including the complete response (CR) and partial response (PR)] and disease control rate [including the CR, PR and stable disease (SD)] from 20 to 60% and 40 to 100%, respectively. Moreover, the objective response rate of the CD3-DSPE-PEG2K-NHS/ATP11B NPs + RT + PD-1 inhibitor group reached 100%, whereas the objective response rate of the RT + PD-1 inhibitor group was only 40% (Fig. 6C). The results of the long-term curative effect analysis (Fig. 6D) indicated that the injection of CD3-DSPE-PEG2K-NHS/ATP11B NPs alone had little effect on the survival of intracranial GBM-bearing mice (median survival time: control group vs. CD3-DSPE-PEG2K-NHS/ATP11B group, 19.00 days vs. 23.00 days, $P = 0.383$); compared with the PD-1 inhibitor group, the survival time of mice in the PD-1 inhibitor + CD3-DSPE-PEG2K-NHS/ATP11B group was significantly prolonged (median survival time: PD-1 inhibitor group vs. PD-1 inhibitor + CD3-DSPE-PEG2K-NHS/ATP11B group, 22.00 days vs. 52.00 days, $P = 0.007$). Notably, among all treatment groups, the RT + PD-1 inhibitor + CD3-DSPE-PEG2K-NHS/ATP11B group demonstrated the most prolonged survival (median survival time: RT + PD-1 inhibitor group vs. RT + PD-1 inhibitor + CD3-DSPE-PEG2K-NHS/ATP11B group, 42.00 days vs. 56.00 days, $P = 0.047$). Collectively, these results suggest that systemic administration of CD3-DSPE-PEG2K-NHS/ATP11B NPs obviously enhances the therapeutic outcomes of RT combined with ICIs in GBM.

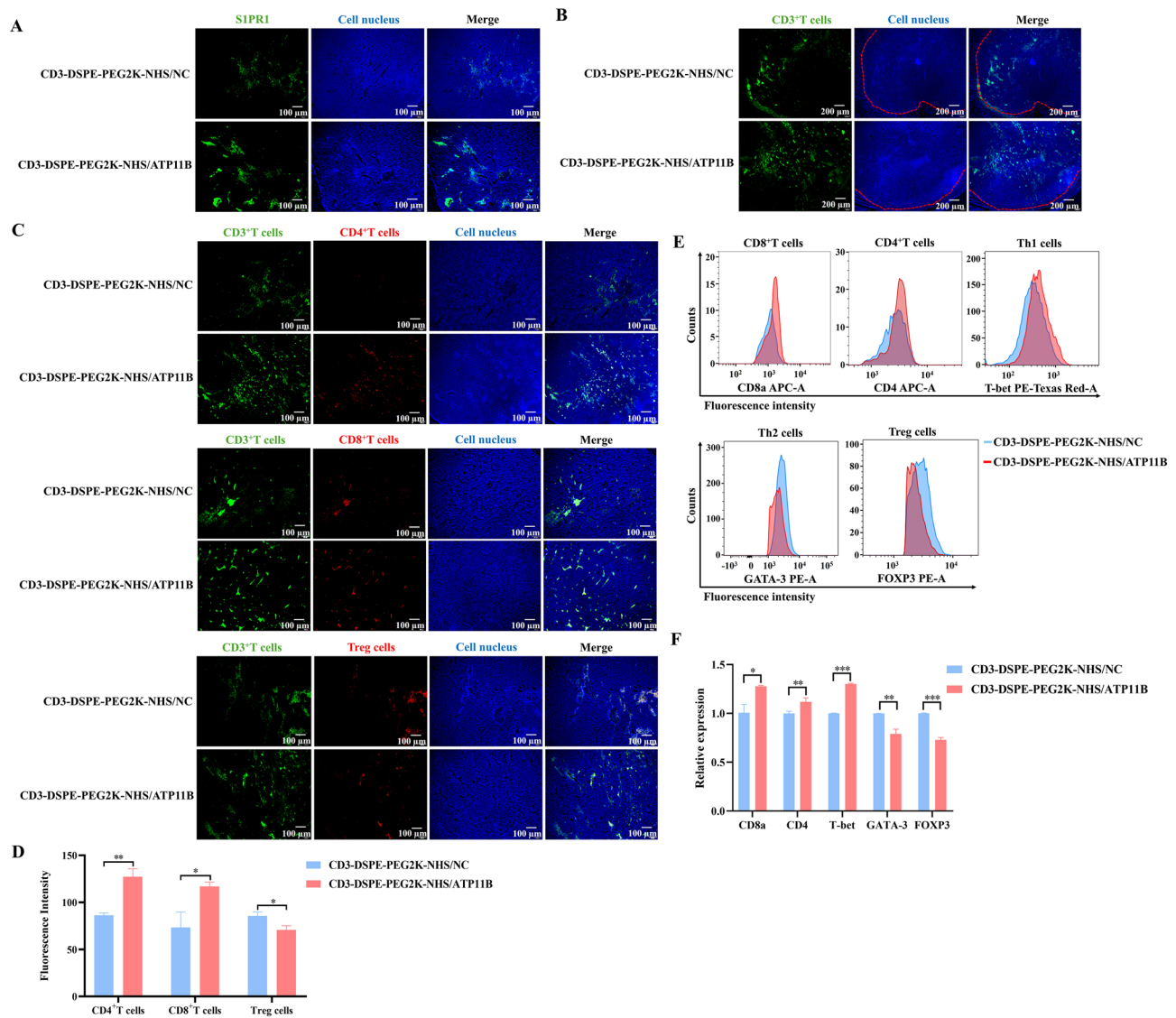


Fig. 5 CD3-DSPE-PEG2K-NHS/ATP11B NPs triggered T cells to infiltrate to GBM and to differentiate towards anti-tumor phenotypes. CD3-DSPE-PEG2K-NHS/ATP11B NPs were injected into intracranial GBM models through the tail vein, and seven days later, brain tissues and peripheral blood samples were collected for detection. **(A)** Immunofluorescence staining of S1PR1 (green) in frozen sections of brain tissues; scale bar: 100 μ m. **(B)** The distribution of T cells (CD3⁺ and green) in frozen brain tissue samples were detected via an immunofluorescence assay. The red dotted line represents the dividing line between normal brain tissue and GBM tissue; blue: cell nucleus; scale bar: 200 μ m. **(C)** The infiltration of CD4⁺ T cells (red), CD8⁺ T cells (red), and Tregs (FOXP3⁺, red) in frozen sections of brain tissues was detected via an immunofluorescence assay; blue: cell nucleus; scale bar: 100 μ m. **(D)** Statistical analysis of three independently repeated datasets derived from C. **(E)** Representative flow cytometry data of CD8⁺ T cells, CD4⁺ T cells, Th1 cells (T-bet⁺), Th2 cells (GATA-3⁺), and Tregs (FOXP3⁺) in peripheral blood samples. **(F)** Statistical analysis of three independently duplicated datasets derived from E

With respect to toxic side effects, we collected several normal organs from the GBM-bearing mice in each group, including the heart, liver, spleen, lung and kidney. The corresponding paraffin sections were prepared, and H&E staining was performed. As shown in Fig. 6E, no visible organ damage was observed in the above tissues, indicating that the CD3-DSPE-PEG2K-NHS/ATP11B NPs combined with the PD-1 inhibitor and RT had no obvious organ toxicity.

Discussion

Among solid malignancies, GBM is highly resistant to ICIs because the particular tumour microenvironment disables the antitumour immune response, and T-cell dysfunction and T-cell lymphopenia are paramount barriers [2, 20, 21]. The main causes of T-cell lymphopenia include excessive death, decreased regeneration, and sequestration in other organs [2, 22, 23]. Chongsathidkiet P et al. reported that the sequestration of T cells in the bone marrow is mediated by the deficiency of externalized S1PR1 on T-cell membranes in patients with brain

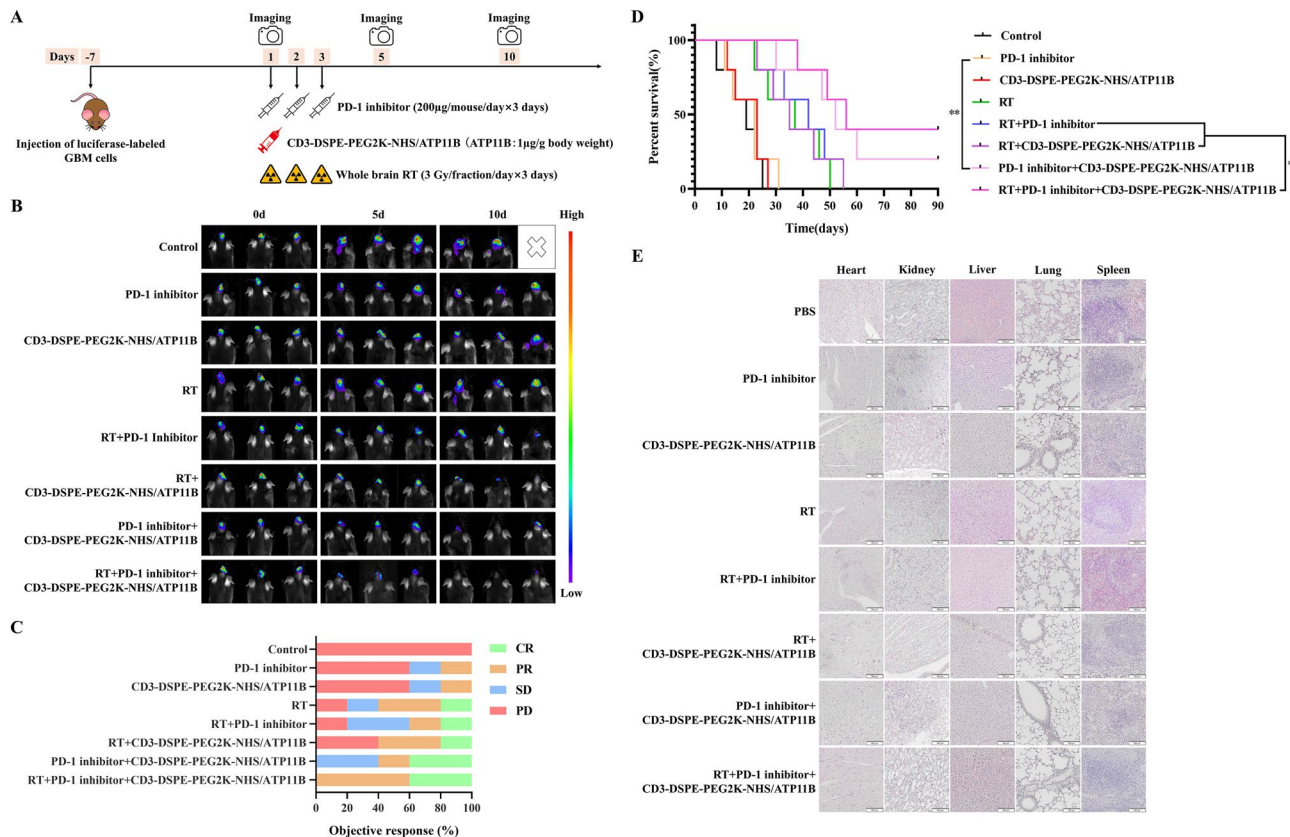


Fig. 6 CD3-DSPE-PEG2K-NHS/ATP11B NPs efficiently enhanced the therapeutic outcomes of RT and ICI with good safety. **(A)** Schematic illustration of the in vivo experimental workflow. **(B)** In vivo bioluminescence imaging of mice bearing intracranial luciferase-labelled GL261 tumours. **(C)** Short-term efficacy evaluation of orthotopic luciferase-labelled GL261-bearing mice in all groups, $n=5$. **(D)** Kaplan–Meier survival curves of orthotopic luciferase-labelled GL261-bearing mice in all groups, $n=5$. **(E)** H&E staining of paraffin sections of heart, kidney, liver, lung, and spleen samples to evaluate the toxicity of CD3-DSPE-PEG2K-NHS/ATP11B NPs combined with a PD-1 inhibitor and RT, $n=3$

tumours [2]. Moreover, S1PR1 inhibition participates in limiting T-cell migration and inducing proapoptotic signaling [4]. Hence, increasing S1PR1 expression and inducing S1PR1 externalization on T cells could enable T cells to egress from the bone marrow and support T-cell survival.

Given that no pharmacologic methods exist for stabilizing or externalizing S1PR1 on the T-cell surface, we attempted to flip internalized S1PR1 to the outside of T-cell membranes with the help of the flippase ATP11B protein. In vitro, we demonstrated that overexpression of the ATP11B protein significantly increased the expression and externalization of S1PR1 on T cells (Fig. 2). More importantly, ATP11B overexpression promoted T lymphocyte differentiation towards antitumour phenotypes and strengthened the ability of T cells to kill GBM cells (Fig. 3), which was consistent with the findings of Chakraborty P et al. [24]. However, many previous studies have shown that highly expressed S1PR1 and ATP11B on cancer cells are involved in inducing cancer progression and treatment resistance [25–30], so artificially overexpressing ATP11B only on T cells, which can be

achieved by specific targeted NPs, is necessary. Here, we synthesized and systemically administered the cationic liposome NPs named CD3-DSPE-PEG2K-NHS/ATP11B into mice bearing intracranial tumours to improve the anti-GBM effects of RT combined with ICIs. Encouragingly, the CD3-DSPE-PEG2K-NHS/ATP11B NPs not only facilitated the egress of T cells into the circulation and home to the GBM but also motivated them to invade the centre of the GBM lesion instead of being distributed around the tumour (Fig. 5B), thereby enhancing the therapeutic outcomes of ICIs alone or in combination with RT in intractable GBM models (Fig. 6).

Notably, the CD3-DSPE-PEG2K-NHS/ATP11B NPs did not have positive effects on RT, either in terms of short-term or long-term efficacy (Fig. 6C and D). We speculate that this may be related to several factors, including the dose and fractionation of RT and the time window for the combination of the CD3-DSPE-PEG2K-NHS/ATP11B NPs and RT. Studies have shown that, compared with conventional fraction schemes which are disadvantageous for RT-induced antitumour immune responses, RT with high-dose per fraction is considered

a preferable therapeutic protocol for enhancing antitumour immune responses through accelerating the release of tumour antigens from cancer cells and enhancing immune presentation [31–34]. To date, the time window between RT and immunotherapy significantly affects therapeutic antitumour responses; however, the optimal schedule has not yet reached consensus, and the administration of immunotherapy initiated before or concurrent with RT may be preferred [35]. In addition, no study has clearly elucidated the specific mechanisms of the internalization of S1PR1 on T cell membranes in populations with primary brain tumours or brain metastases. Previous studies suggested that, compared with normal brain tissue, CD69 expression is increased in GBM tissue [36], the upregulated CD69 can bind to S1PR1 and form the CD69-S1PR1 complex, thereby mediating the internalization of S1PR1 [37]. However, there has been no relevant report on the regulation of S1PR1 expression and membrane localization by ATP11B, although we confirmed that ATP11B promoted the expression and externalization of S1PR1, the molecular mechanisms involved is still unclear now.

In conclusion, the upregulation and externalization of S1PR1 on T cells mediated by targeted overexpression of ATP11B represents a promising therapeutic strategy to ameliorate the immunosuppressive microenvironment and further improve the outcomes of immunotherapies including ICIs in patients with GBM.

Supplementary Information

The online version contains supplementary material available at <https://doi.org/10.1186/s12967-025-06594-0>.

Supplementary Material 1

Acknowledgements

Not applicable.

Author contributions

Hui Qiu: data curation, formal analysis, methodology, writing-original draft, writing-review & editing, funding acquisition. Ziqin Chen: data curation, formal analysis, methodology, writing-original draft. Jie Chen: data curation, formal analysis, methodology, writing-original draft. Huijuan Yu: formal analysis, methodology. Xin Wen: formal analysis, methodology. Chang Xu: data curation. Gongzhen Liu: data curation. Luyijie Chai: data curation. Longzhen Zhang: funding acquisition. Yilong Guo: conceptualization, supervision, writing-review & editing. Xin Ding: conceptualization, supervision, writing-review & editing, funding acquisition.

Funding

This work was supported by National Natural Science Foundation of China (No. 81972845); Introduction of Specialist Team in Clinical Medicine of Xuzhou (No. 2019TD003); Advanced Program of The Affiliated Hospital of Xuzhou Medical University (No. PYJH2024313); Major Project of Basic Science (Natural Science) Research in Higher Education Institutions of Jiangsu Province (No. 24KJA320009).

Data availability

The data are available from the corresponding author on reasonable request.

Declarations

Ethics approval and consent to participate

All procedures involving animals were in compliance with the guidelines of Jiangsu Council on Animal Care, and ethical approval was granted by the animal ethics committee of Xuzhou Medical University of China (No: 2022105005).

Consent for publication

Not applicable.

Competing interests

The authors declare that they have no competing interests.

Received: 13 February 2025 / Accepted: 8 May 2025

Published online: 27 May 2025

References

1. Jansen JA, Omuro A, Lucca LE. T cell dysfunction in glioblastoma: a barrier and an opportunity for the development of successful immunotherapies. *Curr Opin Neurol*. 2021;34(6):827–33. <https://doi.org/10.1097/WCO.0000000000000988>
2. Chongsathidkiet P, Jackson C, Koyama S, Loebel F, Cui X, Farber SH, Woroniecka K, Elsamadicy AA, Dechant CA, Kemeny HR, Sanchez-Perez L, Cheema TA, Souders NC, Herndon JE, Coumans JV, Everitt JL, Nahed BV, Sampson JH, Gunn MD, Martuza RL, Dranoff G, Curry WT, Fecci PE. Sequestration of T cells in bone marrow in the setting of glioblastoma and other intracranial tumors. *Nat Med*. 2018;24(9):1459–68. <https://doi.org/10.1038/s41591-018-0135-2>
3. Wang T, Zhang H, Han Y, Zheng Q, Liu H, Han M, Li Z. Reversing T cell dysfunction to boost glioblastoma immunotherapy by Paroxetine-Mediated GRK2 Inhibition and Blockade of multiple checkpoints through biomimetic nanoparticles. *Adv Sci (Weinh)*. 2023;10(9):e2204961. <https://doi.org/10.1002/adv.202204961>
4. Dixit D, Hallisey VM, Zhu EY, Okuniewska M, Cadwell K, Chipuk JE, Axelrad JE, Schwab SR. S1PR1 Inhibition induces proapoptotic signaling in T cells and limits humoral responses within lymph nodes. *J Clin Invest*. 2024;134(4). <https://doi.org/10.1172/JCI174984>
5. Tian L, Wu Y, Choi HJ, Sui X, Li X, Sofi MH, Kassir MF, Chen X, Mehrotra S, Ogretmen B, Yu XZ. S1P/S1PR1 signaling differentially regulates the allogeneic response of CD4 and CD8 T cells by modulating mitochondrial fission. *Cell Mol Immunol*. 2022;19(11):1235–50. <https://doi.org/10.1038/s41423-022-00921-x>
6. Andersen JP, Vestergaard AL, Mikkelsen SA, Mogensen LS, Chalat M, Molday RS. P4-ATPases as phospholipid Flippases-Structure, function, and enigmas. *Front Physiol*. 2016;7:275. <https://doi.org/10.3389/fphys.2016.00275>
7. Xu J, Su SM, Zhang X, Chan UI, Adhav R, Shu X, Liu J, Li J, Mo L, Wang Y, An T, Lei JH, Miao K, Deng CX, Xu X. ATP11B inhibits breast cancer metastasis in a mouse model by suppressing externalization of nonapoptotic phosphatidylserine. *J Clin Invest*. 2022;132(5). <https://doi.org/10.1172/JCI149473>
8. Zhang Y, Zhang S, Zhao X, Wu P, Ying Y, Wu L, Zhuang J, Chen Z, Chao Y, Dong X, Zhao RC, Wang J. ATP11B Modulates Microglial Lipid Metabolism and Alleviates Alzheimer's Disease Pathology. *MedComm* (2020). 2025;6(4):e70139. <https://doi.org/10.1002/mco2.70139>
9. Pulica R, Aquib A, Varsanyi C, Gadiyar V, Wang Z, Frederick T, Calianese DC, Patel B, de Dios KV, Poalasin V, De Lorenzo MS, Kotenko SV, Wu Y, Yang A, Choudhary A, Sriram G, Birge RB. Dys-regulated phosphatidylserine externalization as a cell intrinsic immune escape mechanism in cancer. *Cell Commun Signal*. 2025;23(1):131. <https://doi.org/10.1186/s12964-025-02090-6>
10. Khare P, Edgecomb SX, Hamadani CM, Tanner EEL. Lipid nanoparticle-mediated drug delivery to the brain. *Adv Drug Deliv Rev*. 2023;197:114861. <https://doi.org/10.1016/j.addr.2023.114861>
11. Metzloff AE, Padilla MS, Gong N, Billingsley MM, Han X, Merolle M, Mai D, Figueroa-Espada CG, Thatte AS, Haley RM, Mukalel AJ, Hamilton AG, Alameh MG, Weissman D, Sheppard NC, June CH, Mitchell MJ. Antigen presenting cell mimetic lipid nanoparticles for rapid mRNA CART cell Cancer immunotherapy. *Adv Mater*. 2024;36(26):e2313226. <https://doi.org/10.1002/adma.202313226>
12. Kheirloomoom A, Kare AJ, Ingham ES, Paulmurugan R, Robinson ER, Baikoghli M, Inayathullah M, Seo JW, Wang J, Fite BZ, Wu B, Tumbale SK, Raie MN,

- Cheng RH, Nichols L, Borowsky AD, Ferrara KW. In situ T-cell transfection by anti-CD3-conjugated lipid nanoparticles leads to T-cell activation, migration, and phenotypic shift. *Biomaterials*. 2022;281:121339. <https://doi.org/10.1016/j.biomaterials.2021.121339>
13. Tilsed CM, Sadiq BA, Papp TE, Areesawangkit P, Kimura K, Noguera-Ortega E, Scholler J, Cerdà N, Aghajanian H, Bot A, Mui B, Tam Y, Weissman D, June CH, Albelda SM, Parhiz H. IL7 increases targeted lipid nanoparticle-mediated mRNA expression in T cells in vitro and in vivo by enhancing T cell protein translation. *Proc Natl Acad Sci U S A*. 2024;121(13):e2319856121. <https://doi.org/10.1073/pnas.2319856121>
14. Zhou JE, Sun L, Jia Y, Wang Z, Luo T, Tan J, Fang X, Zhu H, Wang J, Yu L, Yan Z. Lipid nanoparticles produce chimeric antigen receptor T cells with interleukin-6 knockdown in vivo. *J Control Release*. 2022;350:298–307. <https://doi.org/10.1016/j.jconrel.2022.08.033>
15. Pang L, Guo S, Huang Y, Khan F, Liu Y, Zhou F, Lathia JD, Chen P. Targeting legumain-mediated cell-cell interaction sensitizes glioblastoma to immunotherapy in preclinical models. *J Clin Invest*. 2025. <https://doi.org/10.1172/JCI186034>
16. Gao Y, Zhang M, Wang G, Lai W, Liao S, Chen Y, Ning Q, Tang S. Metabolic cross-talk between glioblastoma and glioblastoma-associated microglia/macrophages: from basic insights to therapeutic strategies. *Crit Rev Oncol Hematol*. 2025;208:104649. <https://doi.org/10.1016/j.critrevonc.2025.104649>
17. Khan F, Pang L, Dunterman M, Lesniak MS, Heimberger AB, Chen P. Macrophages and microglia in glioblastoma: heterogeneity, plasticity, and therapy. *J Clin Invest*. 2023;133(1). <https://doi.org/10.1172/JCI163446>
18. Fermi V, Warta R, Wollner A, Lotsch C, Jassowicz L, Rapp C, Knoll M, Jungwirth G, Jungk C, Dao Trong P, von Deimling A, Abdollahi A, Unterberg A, Herold-Mende C. Effective reprogramming of Patient-Derived M2-Polarized Glioblastoma-Associated microglia/macrophages by treatment with GW2580. *Clin Cancer Res*. 2023;29(22):4685–97. <https://doi.org/10.1158/1078-0432.CCR-23-0576>
19. Deng Y, Chen Q, Wan C, Sun Y, Huang F, Hu Y, Yang K. Microglia and macrophage metabolism: a regulator of cerebral gliomas. *Cell Biosci*. 2024;14(1):49. <https://doi.org/10.1186/s13578-024-01231-7>
20. Zhou S, Huang Y, Chen Y, Liu Y, Xie L, You Y, Tong S, Xu J, Jiang G, Song Q, Mei N, Ma F, Gao X, Chen H, Chen J. Reprogramming systemic and local immune function to empower immunotherapy against glioblastoma. *Nat Commun*. 2023;14(1):435. <https://doi.org/10.1038/s41467-023-35957-8>
21. Ravi VM, Neidert N, Will P, Joseph K, Maier JP, Kuckelhaus J, Vollmer L, Goeldner JM, Behringer SP, Scherer F, Boerries M, Follo M, Weiss T, Delev D, Kernbach J, Franco P, Schallner N, Dierks C, Carro MS, Hofmann UG, Fung C, Sankowski R, Prinz M, Beck J, Salie H, Bengsch B, Schnell O, Heiland DH. T-cell dysfunction in the glioblastoma microenvironment is mediated by myeloid cells releasing interleukin-10. *Nat Commun*. 2022;13(1):925. <https://doi.org/10.1038/s41467-022-28523-1>
22. Saidakova EV. Lymphopenia and Mechanisms of T-Cell Regeneration. *Cell tissue biol*. 2022;16(4):302–11. <https://doi.org/10.1134/S1990519X2204006X>
23. Yang R, Sun L, Li CF, Wang YH, Yao J, Li H, Yan M, Chang WC, Hsu JM, Cha JH, Hsu JL, Chou CW, Sun X, Deng Y, Chou CK, Yu D, Hung MC. Galectin-9 interacts with PD-1 and TIM-3 to regulate T cell death and is a target for cancer immunotherapy. *Nat Commun*. 2021;12(1):832. <https://doi.org/10.1038/s41467-021-21099-2>
24. Chakraborty P, Vaena SG, Thyagarajan K, Chatterjee S, Al-Khami A, Selvam SP, Nguyen H, Kang I, Wyatt MW, Baliga U, Hedley Z, Ngang RN, Guo B, Beeson GC, Husain S, Paulos CM, Beeson CC, Zilliox MJ, Hill EG, Mehrotra M, Yu XZ, Ogretmen B, Mehrotra S. Pro-Survival lipid Sphingosine-1-Phosphate metabolically programs T cells to limit Anti-tumor activity. *Cell Rep*. 2019;28(7):1879–e937. <https://doi.org/10.1016/j.celrep.2019.07.044>
25. Nakano T, Okita K, Okazaki S, Yoshimoto S, Masuko S, Yagi H, Kato K, Tomioka Y, Imai K, Hamada Y, Masuko K, Shimada-Takaura K, Nagai N, Saya H, Arai T, Ishiwata T, Masuko T. CD44v, S1PR1, HER3, MET and cancer-associated amino acid transporters are promising targets for the pancreatic cancers characterized using mAb. *FEBS Open Bio*. 2025. <https://doi.org/10.1002/2211-5463.13963>
26. Wang YQ, Ren Y, Gale RP, Niu LT, Huang XJ. Sphingosine-1 phosphate receptor 1 (S1PR1) expression maintains stemness of acute myeloid leukemia stem cells. *Cancer Lett*. 2024;600:217158. <https://doi.org/10.1016/j.canlet.2024.217158>
27. Tao YP, Zhu HY, Shi QY, Wang CX, Hua YX, Hu HY, Zhou QY, Zhou ZL, Sun Y, Wang XM, Wang Y, Zhang YL, Guo YJ, Wang ZY, Che X, Xu CW, Zhang XC, Heger M, Tao SP, Zheng X, Xu Y, Ao L, Liu AJ, Liu SB, Cheng SQ, Pan WW. S1PR1 regulates ovarian cancer cell senescence through the PDK1-LATS1/2-YAP pathway. *Oncogene*. 2023;42(47):3491–502. <https://doi.org/10.1038/s41388-023-02853-w>
28. Tang T, Huang X, Zhang G, Lu M, Hong Z, Wang M, Huang J, Zhi X, Liang T. Oncolytic peptide LTX-315 induces anti-pancreatic cancer immunity by targeting the ATP11B-PD-L1 axis. *J Immunother Cancer*. 2022;10(3). <https://doi.org/10.1136/jitc-2021-004129>
29. Dong N, Qi W, Wu L, Li J, Zhang X, Wu H, Zhang W, Jiang J, Zhang S, Fu W, Liu Q, Qi G, Wang L, Lu Y, Luo J, Kong Y, Liu Y, Zhao RC, Wang J. LINC00606 promotes glioblastoma progression through sponge miR-486-3p and interaction with ATP11B. *J Exp Clin Cancer Res*. 2024;43(1):139. <https://doi.org/10.1186/s13046-024-03058-z>
30. Xiong X, Zeng L, Zeng F, Huang Y, Jia L. Bioinformatics exploration of the S1PR1 receptor in various human cancers and its clinical relevance. *Discov Oncol*. 2025;16(1):449. <https://doi.org/10.1007/s12672-025-02241-8>
31. Onyshchenko K, Luo R, Rao X, Zhang X, Gaedlicke S, Grosu AL, Firat E, Niedermann G. Hypofractionated radiotherapy combined with Lenalidomide improves systemic antitumor activity in mouse solid tumor models. *Theranostics*. 2024;14(6):2573–88. <https://doi.org/10.7150/thno.88864>
32. Mao L, Zhou JJ, Xiao Y, Yang QC, Yang SC, Wang S, Wu ZZ, Xiong HG, Yu HJ, Sun ZJ. Immunogenic hypofractionated radiotherapy sensitising head and neck squamous cell carcinoma to anti-PD-L1 therapy in MDSC-dependent manner. *Br J Cancer*. 2023;128(11):2126–39. <https://doi.org/10.1038/s41416-023-02230-0>
33. Ma L, Li Y, Sakamoto Y, Xie L, Suzuki S, Yoshida Y, Sui L, Guo G, Wen J, Ren W, Kakimi K, Osada K, Takahashi A, Shimokawa T. Optimal radiation dose to induce an abscopal effect by combining carbon-ion radiotherapy and anti-CTLA4 antibody. *Neoplasia*. 2025;60:101099. <https://doi.org/10.1016/j.neo.2024.101099>
34. Kostopoulos N, Costabile F, Krimtza E, Beghi S, Goia D, Perales-Linares R, Thyfronitis G, LaRiviere MJ, Chong EA, Schuster SJ, Maity A, Koumenis C, Plastaras JP, Facciabene A. Local radiation enhances systemic CAR T-cell efficacy by augmenting antigen crosspresentation and T-cell infiltration. *Blood Adv*. 2024;8(24):6308–20. <https://doi.org/10.1182/bloodadvances.2024012599>
35. Liu Y, Dong Y, Kong L, Shi F, Zhu H, Yu J. Abscopal effect of radiotherapy combined with immune checkpoint inhibitors. *J Hematol Oncol*. 2018;11(1):104. <https://doi.org/10.1186/s13045-018-0647-8>
36. Nisnboym M, Sneiderman CT, Jaswal AP, Xiong Z, Vincze SR, Sever RE, Zou H, Frederico SC, Agnihotri S, Hu B, Drappatz J, Pollack IF, Kohanbash G, Raphael I. Assessment of anti-CD69 antibody therapy alone or in combination with anti-PD-1 in murine GBM. *Expert Rev Clin Immunol*. 2025;21(2):239–47. <https://doi.org/10.1080/1744666X.2024.2412770>
37. Chen H, Qin Y, Chou M, Cyster JG, Li X. Transmembrane protein CD69 acts as an S1PR1 agonist. *Elife*. 2023;12. <https://doi.org/10.7554/eLife.88204>

Publisher's note

Springer Nature remains neutral with regard to jurisdictional claims in published maps and institutional affiliations.